

Article

Winding Hottest-Spot Temperature Analysis in Dry-Type Transformer Using Numerical Simulation

Rafael Gonçalves Mafra ¹, Elisan dos Santos Magalhães ¹ , Bruno de Campos Salles Anselmo ¹, Fernando Nunes Belchior ² and Sandro Metrevelle Marcondes Lima e Silva ^{1,*} 

¹ Heat Transfer Laboratory—LabTC, Institute of Mechanical Engineering—IEM, Federal University of Itajubá—UNIFEI, Campus Prof. José Rodrigues Seabra, Av. BPS, 1303, 37500-903 Itajubá, MG, Brazil; mafra534@gmail.com (R.G.M.); elisan@unifei.edu.br (E.d.S.M.); brunocsa@gmail.com (B.d.C.S.A.)

² Faculty of Science and Technology, Federal University of Goiás, Mucuri Street, 920, Itatiaia Park, 74968-755 Aparecida de Goiânia, GO, Brazil; fnbelchior@hotmail.com

* Correspondence: metrevell@unifei.edu.br; Tel.: +55-35-3629-1069

Received: 6 September 2018; Accepted: 25 September 2018; Published: 26 December 2018



Abstract: A thermal analysis of a 5 kVA dry-type transformer under linear and non-linear loads conditions is studied in this paper. The main goal here is to calculate the hottest-spot transformer temperature under free convection through the resolution of the heat conduction equation in three dimensions (3D) using COMSOL Multiphysics[®]. The proposed technique was validated through experimental data obtained in laboratory. The temperature inside the cores was measured under the influence of free convection. The radiation emission was also measured through a thermal camera. The heat transfer coefficient for both conditions was obtained from empirical correlations. The hottest-spot temperatures were determined from the analysis in the commercial software which was used for the numerical simulations of the transformer heating and cooling under some loading conditions. The temperature residuals, that is, the experimental temperature values subtracted by the numerical temperature values, were below 10%. The numerical analysis found that the hottest-spot temperatures in the core reached 20 °C above the transformer insulation limit. The location of the hottest-spot as well as the obtained temperatures can be used to improve more resistant dry-type transformers.

Keywords: hottest-spot temperature; free convection; dry-type transformer; COMSOL Multiphysics[®]

1. Introduction

Due to current technological developments, the quality of electrical energy distribution has become an important concern in many pieces of electrical equipment. In fact, the nature of the loads has changed over the years; electronic equipment has become more sensitive to fluctuations, thus requiring a higher quality energy supply [1]. A key component in an electrical transmission/distribution system is the transformer. As the majority of the transformers are used in non-linear operation conditions, they should be projected to transfer dynamic loads as effectively as possible. Likewise, the transformers should operate at the maximum capacity without reaching their thermal limit. This will obviously increase the cost-effectiveness of the transformer [2].

There are mainly two types of transformers: The oil-filled type and the cast-resin dry-type, which is one of the commonly most used types of transformers. This one has an advantage over the oil-filled transformers mostly due to the flammability and moisture issues. However, the temperature increase in this device is related to the type of resin used [3]. The rise of temperature in the transformer is related to the internal losses. The higher the temperature reaches, the lower the transformer lifespan.

Therefore, to optimize a transformer, it is essential to identify the critical areas which present the highest temperatures. Those areas are commonly called the hottest-spots.

In recent years, a substantial amount of research has been conducted to predict the winding hottest-spot temperature (HST). A common hottest-spot thermal model is provided in the IEEE manual [4], commonly referred to as the clause 7 model. Many authors have proved its viability [5–7]. Besides the clause 7 model, many authors have proposed models for predicting the HST. For instance, Swift et al. [8] developed a methodology to consider a similar circuit to illustrate the heat transference in transformers. Susa et al. [9,10] proposed a more accurate thermal model for the HST in transformers working in dynamic load conditions. These authors' proposal relies on the heat transfer study, the lumped capacitance assumption, the thermal electrical relation, and the non-linear thermal resistance concept. Smolka and Nowak [11] proposed a coupled heat transfer and electromagnetic computational code for a cast resin transformer. Their model was capable of predicting the temperature distribution and analyzing its surroundings very accurately.

Another option to study the heat transfer behavior in a transformer is the use of the finite element method (FEM) to solve the heat diffusion equations. For instance, Lee et al. [12] analyzed the temperature effects of the air surroundings in the cooling process of the windings using the FEM to solve the two-dimensional heat diffusion equation. Eslamian et al. [13] have applied the aforementioned method to obtain the capacitance and inductances of dry-type transformers. Ning and Ding [14] applied the FEM analysis to model the temperature field of the fluid in a dry-type transformer. In the present work, COMSOL (COMSOL Ltd.a, Curitiba, Paraná, Brazil) was used to model the thermal field contours and winding temperature rising. Tsili et al. [15] analyzed an oil-immersed power transformer by using the three-dimensional heat transfer model, Navier-Stokes and Boussinesq equations through a CFD analysis. Li et al. [16] evaluated the behavior of the temperature in amorphous core dry-type transformers using a three-dimensional FEM to determine how temperature varies in the iron core and winding. Bulnes et al. [17] proposed a model to predict the heat flow under permanent and variable load conditions.

In order to determine the thermal field in dry-type transformer windings, the three-dimensional heat diffusion equation was solved in the software. This methodology enabled the determination of the core hottest spot temperature. Therefore, from the determination of the temperature value of these hotspots, it is possible to better understand the problems that lead to transformer malfunction due to temperature excess. Thus, besides being a less expensive and a more accurate way to find the hottest spot and study the thermal behavior of dry-type transformers, this methodology also allows the optimization of dry-type transformers. The key point in the work is the transformer analysis using a multi-geometrical software. The effect of the heat diffusion was solved in two coordinate systems which is adaptable to the predominant geometry of the core and windings. The details on the geometrical assembly, windings, Kraft paper, and iron silicon core are not currently found in the literature. Furthermore, the numerical analysis is validated with experiments, which proves the accuracy of the analyzed model.

2. Methodology

2.1. Thermal Model

The FEM was used in the commercial software used in this work to work out the unsteady 3D heat conduction equation with internal generation and to learn how the temperature distributes in the core. Figure 1 presents a representation of the adopted conditions in the transformer core. The core is subjected to an internal heat generation \dot{q} , heat losses by convection and radiation and it is immersed in a medium with T_∞ temperature.

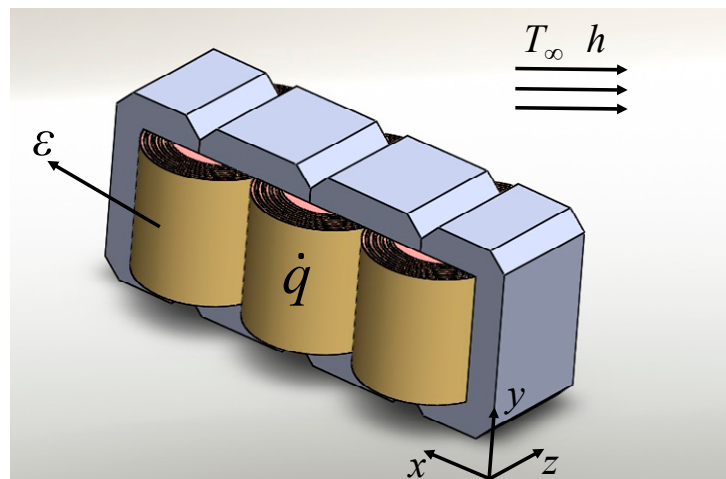


Figure 1. Representation of the thermal model of the core.

To acquire the heat variation in the core, the 3D heat conduction equation with internal heat generation is divided in two geometries. In the first one, the iron core is modeled in Cartesian coordinates (gray region in Figure 1). The heat diffusion equation for constant thermal properties for this case is given by:

$$\frac{\partial^2 T}{\partial x^2} + \frac{\partial^2 T}{\partial y^2} + \frac{\partial^2 T}{\partial z^2} + \frac{\dot{q}}{k} = \frac{\rho c_p}{k} \frac{\partial T}{\partial t} \quad (1)$$

where k is thermophysical conductivity, ρ is the density, c_p is the specific heat, T is the temperature, t is the time, and x , y and z are the coordinates. In the second case, for the cylindrical region (copper windings in Figure 1), the three-dimensional heat diffusion equation was modeled in cylindrical coordinates with constant thermal properties. This equation is given by:

$$\frac{1}{r} \frac{\partial}{\partial r} \left(r \frac{\partial T}{\partial r} \right) + \frac{1}{r^2} \frac{\partial^2 T}{\partial \phi^2} + \frac{\partial^2 T}{\partial z^2} + \frac{\dot{q}}{k} = \frac{\rho c_p}{k} \frac{\partial T}{\partial t} \quad (2)$$

where r and ϕ are the cylindrical coordinates.

Convection and radiation limit conditions were applied to external surfaces of the transformer core. Those boundary conditions are given by Equation (3).

$$-k \frac{\partial T}{\partial \eta} = h(T - T_\infty) + \sigma \varepsilon (T^4 - T_\infty^4) \quad (3)$$

in which η is the normal course, ε is the emissivity and σ is the Stefan-Boltzmann constant.

The initial condition of uniform temperature was also applied in $t = 0$ s. In this case, the initial temperature of the core was the same as room temperature.

2.2. Correlations for Free Convection

The average convective coefficient (\bar{h}) of the iron silicon part was obtained from the empirical correlations from Barroso [18]. First, Barroso determined the Nusselt number Nu_L for the vertical plate (side of the iron silicon part) and then the Nu_U and Nu_l for the upper and lower horizontally positioned plate. The correlations for Nu_L , Nu_U and Nu_l are given by:

$$Nu_L = \left(\frac{0.825 + 0.387 Ra^{1/6}}{\left(1 + \left(\frac{0.492}{Pr} \right)^{9/16} \right)^{8/27}} \right)^2 \quad (4)$$

$$Nu_U = 0.15Ra^{1/3} \quad (5)$$

$$Nu_D = 0.27Ra^{1/4} \quad (6)$$

where the Rayleigh number Ra , Prandtl number Pr , and Nusselt number Nu_L are applied on the side of the iron silicon part, Nu_U is applied on the upper surface, and Nu_D is applied on the bottom side of the sample.

On the winding modeling, the heat transfer coefficient was obtained from empirical correlations for a cylinder obtained in Rahimpour and Azizian [19]. The correlation is given by:

$$Nu_c = \left(\frac{4Pr^2Gr}{36 + 45Pr} \right)^{1/5} \quad (7)$$

where Nu_c is the Nusselt number for the winding side, and Gr is the Grashoff number. Equation (8) is used to obtain \bar{h} :

$$\bar{h} = \frac{k_{air} Nu}{L_c} \quad (8)$$

where the thermal conductivity of the air is represented by k_{air} , and the characteristic length of the side is represented by L_c .

2.3. Numerical Solution

The thermal conductivity and thermal diffusivity values depend on the type of core materials, which are copper, Kraft paper, and iron silicon. Figure 2 presents details of the simulated assembly. Figure 2a presents the iron silicon part of the core. It is composed of a four-divided part where the windings are placed. Figure 2b presents details of the Kraft paper placed between each layer of the winding.

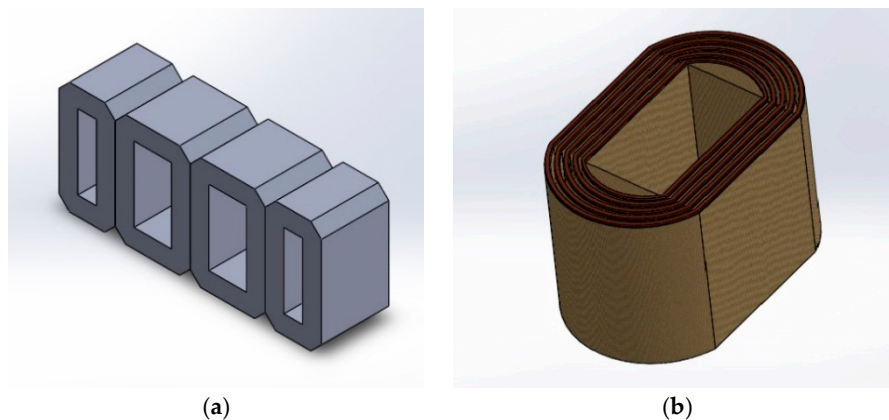


Figure 2. (a) Iron silicon part and (b) details on the paper and cooper winding.

As presented by Bergman et al. [20], the thermal conductivity of copper and iron silicon may be considered constant in the temperature range. The Kraft paper has stable thermal conditions in the temperature range of 0 to 200 °C, as in Liao et al. [21]. Therefore, the thermal properties of the Kraft paper may also be regarded as constant. From Bergman et al. [20], the thermal conductivity was considered to be 400 W/mK for the copper, 0.089 W/mK for the Kraft paper and 45.0 W/mK for the iron silicon. The thermal diffusivity was considered to be $119.42 \times 10^{-6} \text{ m}^2/\text{s}$ for the copper, $0.07417 \times 10^{-6} \text{ m}^2/\text{s}$ for the Kraft paper and $17.58 \times 10^{-6} \text{ m}^2/\text{s}$ for the iron silicon. The simulation assumed a perfect contact between the assembly parts. Therefore, the thermal contact resistance was disregarded. The simulation also considered that the insulation losses, such as partial discharges, polarization and moisture, are negligible when compared to the core and winding losses.

The mesh applied in the simulation has tetrahedral elements. This type of elements was chosen due to the better adaptability to the complex core geometry. Figure 3a shows a detailed view of the contact between the cooper winding and iron silicon part. Figure 3b presents the generated mesh with 1,764,912 elements.

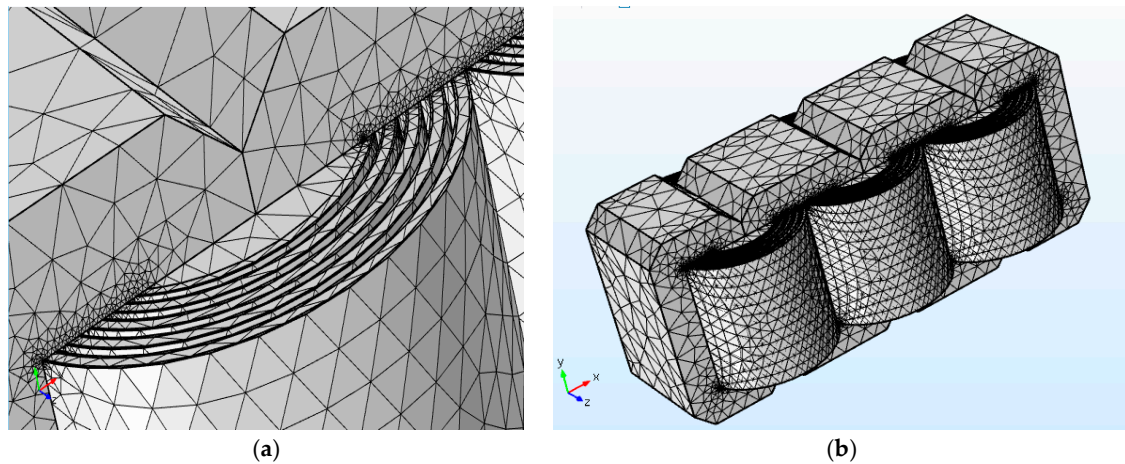


Figure 3. (a) Detail of the cooper winding and iron silicon contact and (b) tetrahedral mesh.

The mesh size was chosen from a mesh refinement test. Table 1 presents the test refinement results. The average temperature on winding 2 was chosen as refinement parameter. As presented, due to the increase of simulation time, the mesh with 1,745,736 tetrahedral elements was chosen.

Table 1. Mesh refinement test.

Test	Number of Tetrahedral Elements	Winding 2 Temperature (°C)	Simulation Time (min)
A1	258,617	127.35	196
A2	545,271	129.6	371
A3	875,452	135.56	562
A4	1,364,912	135.88	891
A5	1,745,736	135.99	1274

3. Experimental Procedure

Figure 4 presents the experimental bench used for the load test. The Agilent 34970A data acquisition system (Keysight Technologies Medicao Brasil LTDA, Barueri, São Paulo, Brazil) was connected to a computer. The three-phase dry-type transformer developed by Orteng has a nominal power of 5 kVA and standard NBR 10295. It is powered with 220 V. The transformer has a thermal class B, which means that the windings may achieve temperatures up to 130 °C without compromising the insulation lifespan.

Three experiments were performed for each condition in order to assure the repeatability of the results. Two conditions were tested, one with linear load and another with dynamic load. Each experiment lasted approximately 25 h. 1500 temperature points were collected in a time interval of 1 min. The transformer reached the steady state when it reached approximately 11.6 h of testing. 4 type J thermocouples were placed in the critical points of the transformer. The temperatures were collected using the Agilent 34970A data acquisition system. The thermocouple locations are presented in Figure 5. Table 2 presents the thermocouple coordinate according to Figure 5.

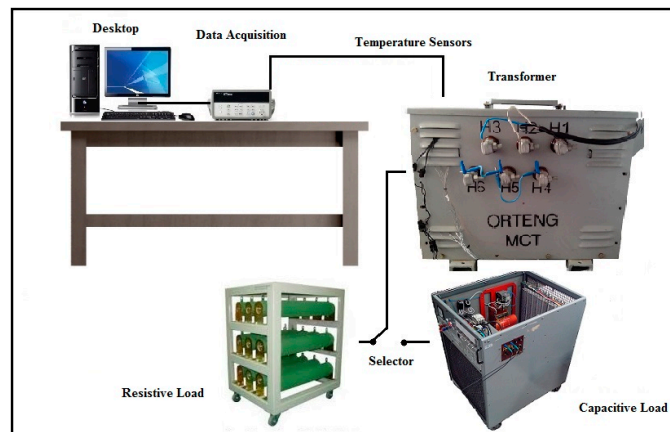


Figure 4. Experimental apparatus.

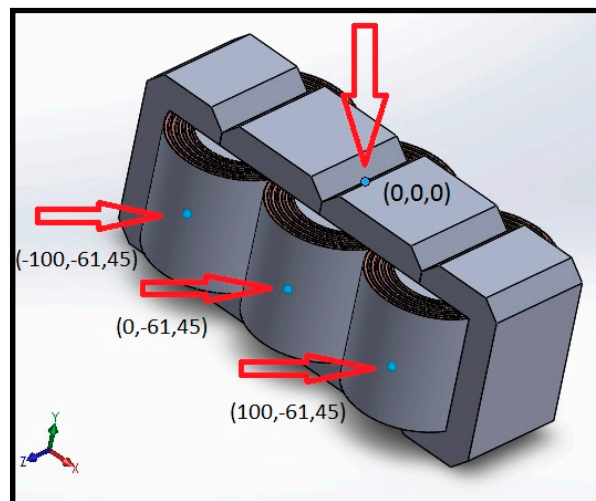


Figure 5. Thermocouple locations.

Table 2. Thermocouple locations.

Thermocouple	Position	Coordinates (mm)
T_1	Winding 1	(−100, −61, 45)
T_2	Winding 2	(0, −61, 45)
T_3	Core surface	(0, 0, 0)
T_4	Winding 3	(100, −61, 45)

The room temperature was kept constant during the tests using air conditioning. The external temperature was maintained at 21 °C for all experimental conditions. The internal heat generation was 205,770.49 W/m³ for the linear case and 457,801.93 W/m³ for the dynamic case. The average convection heat transfer coefficients were 6.49 W/m²K for the linear load and 6.83 W/m²K for the dynamic load. The emissivity value of 0.9 was experimentally measured with a FLIR T450SC (FLIR Systems Brazil, Sorocaba, São Paulo, Brazil) according to the procedure described by Magalhães et al. [22].

4. Result Analysis

Figure 6 presents the experimental temperature values obtained for the linear and dynamic load cases. For both cases, the hottest temperature measured was expressed by sensor T_2 . In the linear load condition, the maximum temperature of 112.5 °C was obtained in the end of the heating period, $t = 712$ min (Figure 6a). Likewise, sensor T_2 achieved 134.2 °C in $t = 573$ min (Figure 6b) for the dynamic

load condition. Indeed, it is expected that the central winding achieves the highest temperature. Due to the symmetrical assembly, windings 1 and 3 should also present similar behavior for the temperatures measured. As presented in Figure 6a,b, sensors T_1 and T_4 exhibit similar temperature curves. Since the core does not have internal heat generation, the lower temperature curve, T_4 is obtained in it.

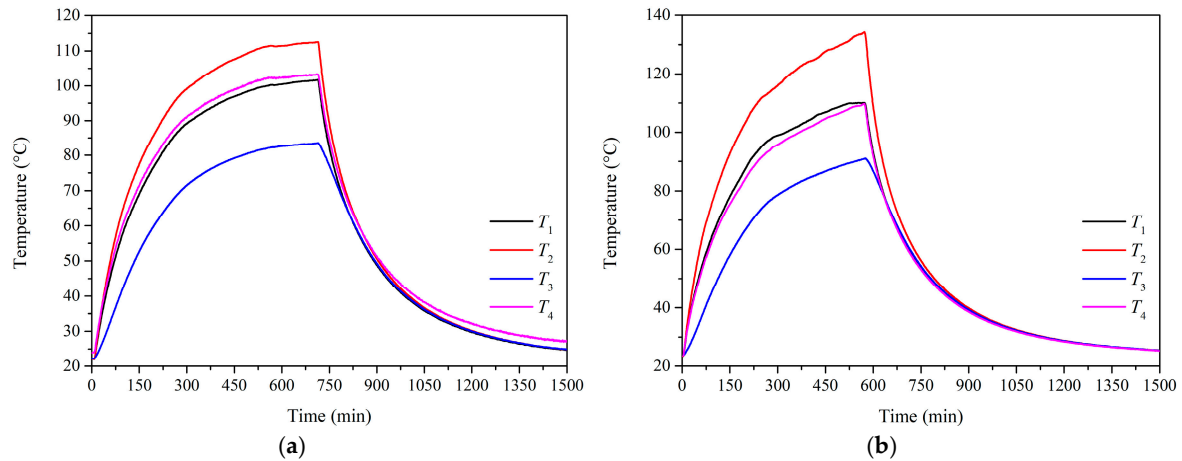


Figure 6. Experimental temperatures for the (a) linear load condition and (b) dynamic load condition.

The dynamic load induced higher temperatures in the transformer windings. Indeed, the average temperature values for the dynamic load were 20% higher than for the linear load.

Figure 7 presents the thermal field for the linear load condition. As can be seen, higher temperatures are closer to the center of the windings. Due to the high losses in windings, the temperatures in the iron silicon are lower than in windings. The only cooling effect considered is due to the free convection. This condition presented a critical heating in the winding. It is worth noting that the transformer has a thermal class B, and for temperatures higher than 130 °C, there is a compromise of the insulation lifespan.

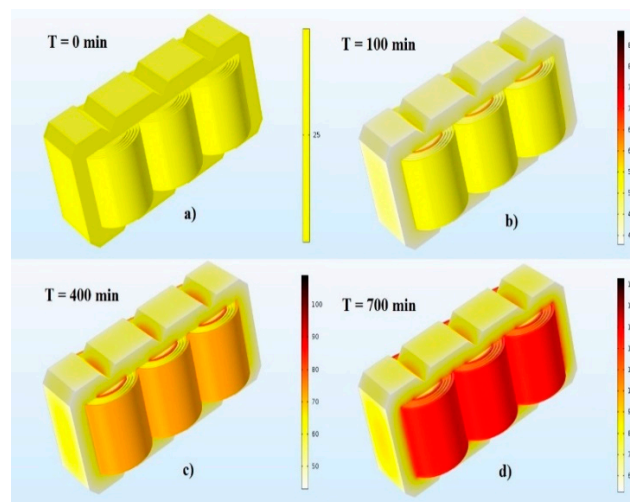


Figure 7. Transformer thermal field for (a) 0 min, (b) 100 min, (c) 400 min, and (d) 700 min.

Figure 8 presents a comparison between the measured and calculated temperatures. As mentioned, the calculated temperatures were acquired from the commercial software used in this work. This comparison is done with temperature sensor T_2 , which presented the highest temperature for both tested conditions. Figure 8a presents the results for the linear load condition, and Figure 8b for the dynamic load condition. Notice that the linear load case presented a better agreement between the

simulated and experimental curves than the dynamic load case. The temperature difference presented in Figure 8b is mainly related to the non-linear characteristic of the dynamic case.

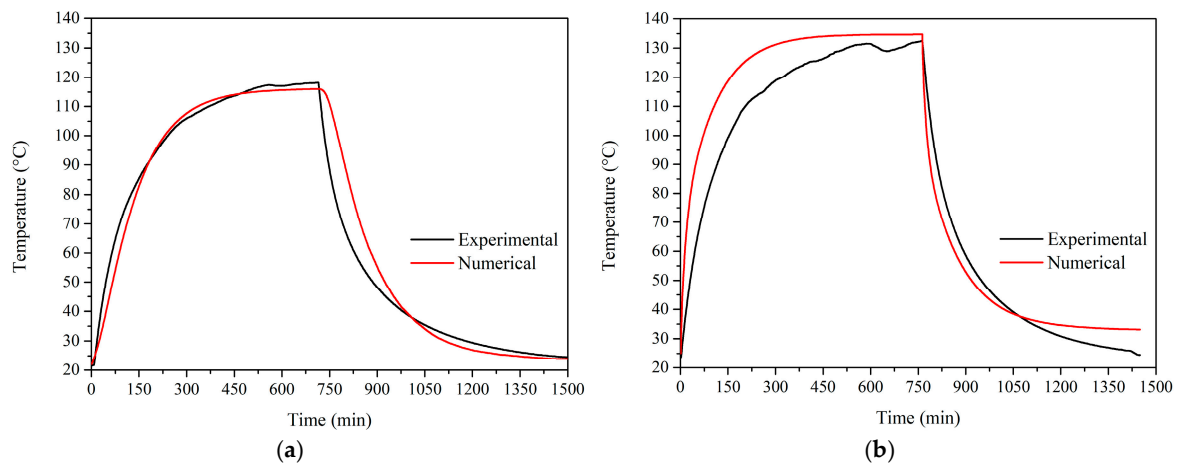


Figure 8. Comparison between numerical and experimental temperatures for (a) linear load and (b) dynamic load.

In order to compare both results, Figure 9 presents the temperature residuals for both conditions. The temperature residuals are the experimental temperature values subtracted by the numerical temperature values. For the linear case (Figure 9a), the maximum temperature difference was about 25 °C at the end of the heating period. On the other hand, the dynamic case had its maximum temperature difference at the beginning of the experiment (Figure 9b). It's worth mentioning that the temperature obtained from sensor T_2 , in the simulation, reached a maximum of 134.78 °C while the detected hotspot temperature was 153.29 °C.

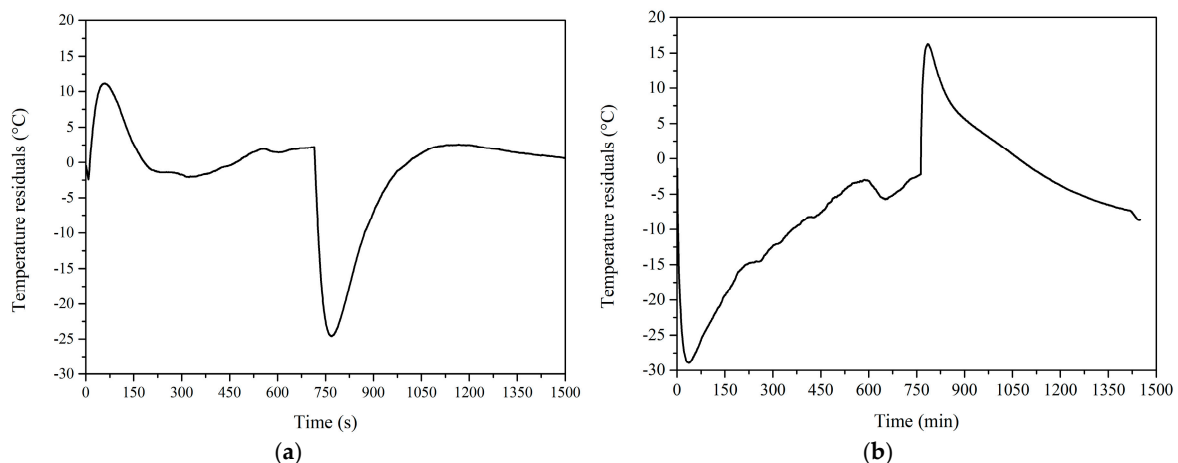


Figure 9. Temperature residuals for (a) linear case and (b) dynamic case.

The software was used to determine the hotspots for both simulated conditions. Table 3 presents the maximum temperatures achieved in the windings on simulation and their corresponding coordinate. The linear case presented a hotspot of 109.25 °C, which classifies the tested transformer as adequate to be used in this condition. As presented in Figure 8b, the dynamic case presented a higher temperature. For this case, the hotspot obtained in the simulation was 153.29 °C. The transformer was projected to withstand temperatures in the order of 130 °C, which undermines its use for dynamic load. It is worth mentioning that a simple thermocouple experiment may not detect the hotspot and compromise the transformer lifespan. Therefore, a numerical analysis is important to detect the

hotspot. Figure 10 presents the thermal distribution of the transformer core with the indication of the hotspot point.

Table 3. Hotspot determination for the analyzed cases.

Load	Temperature (°C)	Coordinates (mm)
Linear	109.25	(102.5, −63.43, 0.63)
Dynamic	153.29	(103, −63.43, 0.63)

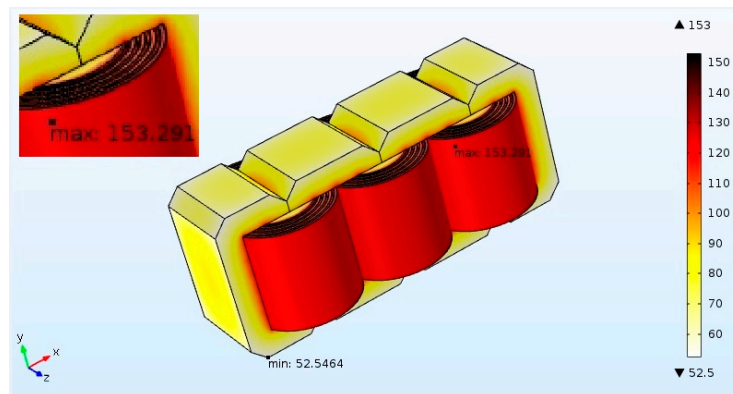


Figure 10. Thermal field and hotspot location for the dynamic case.

From the analysis of Figure 10, it may be inferred that highest temperatures occur closer to the upper surface in the middle phase of the windings. This indicates that to reduce the hottest-spot temperature a cooling system could be positioned in this area. This cooling system could induce a higher heat transfer convection coefficient, therefore reducing the temperature. Preliminary analysis of this configuration indicates there is a cost-benefit relationship between the cost to maintain the cooling system and the expected increase of transformer lifespan.

Figure 11 presents the thermal field obtained through an infrared sensor for the linear case. It can be noted that the lower temperature is in the iron core, as predicted in the numerical simulation. It may be seen that the temperature, in the measured point in Figure 11c, reaches 108 °C. This temperature approaches the measured temperature when the experiment achieves the permanent condition (Figure 8a).

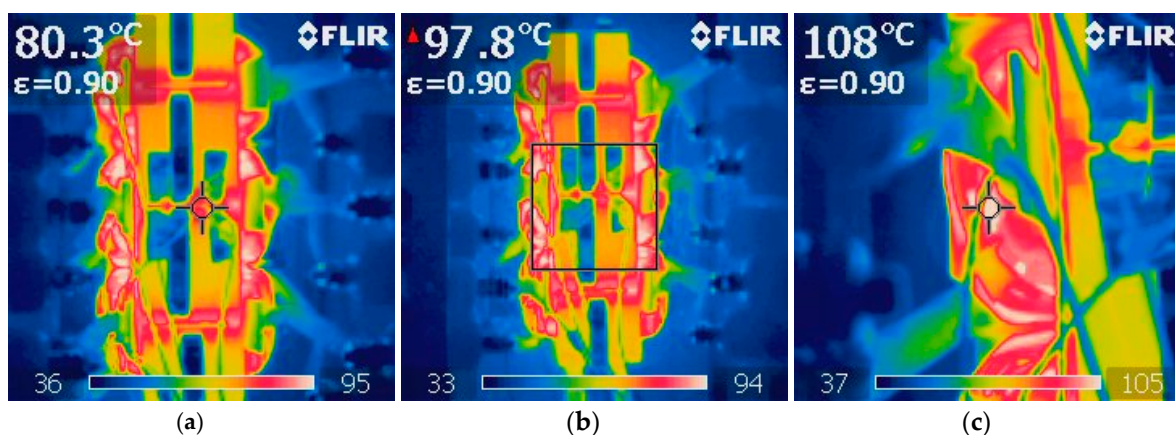


Figure 11. Thermal pictures for (a) thermal core temperature, (b) average temperature region and (c) temperature in windings.

5. Conclusions

This work proposed a methodology for the hotspot determination of a 5 kVA dry-type transformer in linear and dynamic loads conditions. The proximity of the simulated and experimental temperature data validated the proposed methodology. The dynamic load case presented a higher temperature than the linear load case. The simulated transient analysis reveals that the measurement of single points of the transformers cannot detect the hotspot. The numerical analysis, however, made this identification possible. The coupling between numerical correlations for the heat transfer coefficient, emissivity radiation determination and the commercial software used in this work made this analysis possible. This study is designed to improve the convective coefficient in dry-type transformers through forced convection.

Author Contributions: R.G.M. developed the methodology used in this manuscript; E.d.S.M. helped R.G.M. with the numerical analysis and wrote the article; B.d.C.S.A. helped R.G.M. to develop the experimental procedure; F.N.B. is a specialist in electrical power systems and was the co-advisor of this work and S.M.M.L.e.S. is a specialist in heat transfer and was the advisor of this work. R.G.M.

Funding: This research was funded by FAPEMIG, CNPq, CAPES and the Institute of Mechanical Engineering of UNIFEL.

Acknowledgments: The authors appreciate the sponsoring from FAPEMIG, CNPq, CAPES and the Institute of Mechanical Engineering of UNIFEL.

Conflicts of Interest: The authors affirm this is an original manuscript.

References

1. Daut, I.; Syafruddin, H.S.; Ali, R.; Samila, M.; Haziah, H. The effects of harmonic components on transformer losses of sinusoidal source supplying non-linear loads. *Am. J. Appl. Sci.* **2006**, *3*, 2131–2133. [[CrossRef](#)]
2. Amoda, O.A.; Tylavsky, D.J.; McCulla, G.A.; Knuth, W.A. Acceptability of three transformer hottest-spot temperature models. *IEEE Trans. Power Deliv.* **2012**, *27*, 13–22. [[CrossRef](#)]
3. Sun, X.; Mu, Z. Analysis of hottest-spot temperature distribution in cast-resin dry-type transformer design. *Adv. Mater. Res.* **2012**, *538–541*, 1015–1019. [[CrossRef](#)]
4. Vinet, L.; Zhedanov, A. *IEEE Guide for Loading Mineral-Oil-Immersed Transformers and Step-Voltage Regulators*; IEEE: Piscataway, NJ, USA, 2011. [[CrossRef](#)]
5. Pierce, L.W. Predicting liquid filled transformer loading capability. *IEEE Trans. Ind. Appl.* **1994**, *30*, 170–178. [[CrossRef](#)]
6. Zodeh, O.M.; Whearty, R.J. Thermal characteristics of a meta-aramid and cellulose insulated transformer at loads beyond nameplate. *IEEE Power Eng. Rev.* **1997**, *17*, 49–50. [[CrossRef](#)]
7. Swift, G.W.; Zocholl, S.E.; Bajpai, M.; Burger, J.F.; Castro, C.H.; Chano, S.R.; Cobelo, F.; De Sa, P.; Fennell, E.C.; Gilbert, J.G.; et al. Adaptive transformer thermal overload protection. *IEEE Trans. Power Deliv.* **2001**, *16*, 516–521. [[CrossRef](#)]
8. Swift, G.; Molinski, T.S.; Lehn, W. A fundamental approach to transformer thermal modeling—Part I: Theory and equivalent circuit. *IEEE Trans. Power Deliv.* **2001**, *16*, 171–175. [[CrossRef](#)]
9. Susa, D.; Lehtonen, M.; Nordman, H. Dynamic thermal modelling of power transformers. *IEEE Trans. Power Deliv.* **2005**, *20*, 197–204. [[CrossRef](#)]
10. Susa, D.; Lehtonen, M. Dynamic thermal modeling of power transformers: further development—Part II. *IEEE Trans. Power Deliv.* **2006**, *21*, 1971–1980. [[CrossRef](#)]
11. Smolka, J.; Nowak, A.J. Experimental validation of the coupled fluid flow, heat transfer and electromagnetic numerical model of the medium-power dry-type electrical transformer. *Int. J. Therm. Sci.* **2008**, *47*, 1393–1410. [[CrossRef](#)]
12. Lee, M.; Abdullah, H.A.; Jofriet, J.C.; Patel, D.; Fahrioglu, M. Air temperature effect on thermal models for ventilated dry-type transformers. *Electr. Power Syst. Res.* **2011**, *81*, 783–789. [[CrossRef](#)]
13. Eslamian, M.; Vahidi, B.; Hosseinian, S.H. Analytical calculation of detailed model parameters of cast resin dry-type transformers. *Energy Convers. Manag.* **2011**, *52*, 2565–2574. [[CrossRef](#)]

14. Ning, W.; Ding, X. Three-dimensional finite element analysis on fluid thermal field of dry-type transformer. In Proceedings of the 2012 Second International Conference on Instrumentation, Measurement, Computer, Communication and Control, Harbin, China, 8–10 December 2012; pp. 516–519.
15. Tsili, M.A.; Amoiralis, E.I.; Kladas, A.G.; Souflaris, A.T. Power transformer thermal analysis by using an advanced coupled 3D heat transfer and fluid flow FEM model. *Int. J. Therm. Sci.* **2012**, *53*, 188–201. [[CrossRef](#)]
16. Li, Y.; Guan, Y.J.; Li, Y.; Li, T.Y. Calculation of thermal performance in amorphous core dry-type transformers. *Adv. Mater. Res.* **2014**, *986–987*, 1771–1774. [[CrossRef](#)]
17. Bulnes, F.; Tello, A.R.; Livera, M. Heat flux analysis in electrical transformers through integral operators of mechanics. *Mod. Mech. Eng.* **2014**, *4*, 84–107. [[CrossRef](#)]
18. Barroso, R. Simulation and experimental validation of the core temperature distribution of a three-phase transformer. In Proceedings of the 2014 COMSOL Conference, Curitiba, Brasil, 23 October 2014.
19. Rahimpour, E.; Azizian, D. Analysis of temperature distribution in cast-resin dry-type transformers. *Electr. Eng.* **2007**, *89*, 301–309. [[CrossRef](#)]
20. Bergman, T.L.; Lavine, A.S.; Incropera, F.P.; DeWitt, D.P. *Fundamentals of Heat and Mass Transfer*; John Wiley & Sons: Hoboken, NJ, USA, 2011.
21. Liao, R.; Zhang, F.; Yang, L. Electrical and thermal properties of kraft paper reinforced with montmorillonite. *J. Appl. Polym.* **2012**, *126*, E291–E296. [[CrossRef](#)]
22. Magalhaes, E.D.; Silva, C.P.; Lima e Silva, A.L.; Lima e Silva, S.M. An alternative approach to thermal analysis using inverse problems in aluminum alloy welding. *Int. J. Numer. Methods Heat Fluid Flow* **2017**, *27*, 561–574. [[CrossRef](#)]



© 2018 by the authors. Licensee MDPI, Basel, Switzerland. This article is an open access article distributed under the terms and conditions of the Creative Commons Attribution (CC BY) license (<http://creativecommons.org/licenses/by/4.0/>).